Materials Chemistry and Physics 200 (2017) 70–77

Contents lists available at ScienceDirect

Materials Chemistry and Physics

journal homepage: www.elsevier.com/locate/matchemphys

Can a light harvesting material be always common in photocatalytic and photovoltaic applications?

Prasenjit Kar, Tuhin Kumar Maji, Jayita Patwari, Samir Kumar Pal*

Department of Chemical, Biological and Macromolecular Sciences, S. N. Bose National Centre for Basic Sciences, Block JD, Sector III, SaltLake, Kolkata 700 106, India

HIGHLIGHTS

- Developed light harvesting nano-hybrid i. e Protoporphyrin IX on TiO_2.
- Cu(II) metalation of PPIX enhanced photocatalytic activity of nanohybrid.
- Cu(II) metalation of PPIX decreased photovoltaic efficiency of nanohybrid.
- Excited state dynamical processes were investigated by ultrafast spectroscopy.

GRAPHICAL ABSTRACT

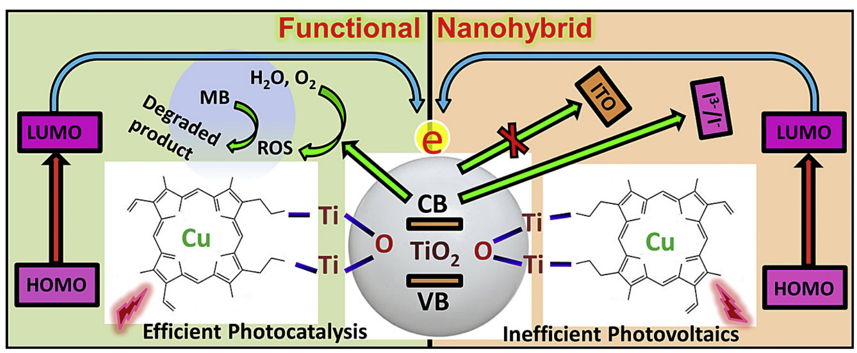

ARTICLE INFO

Article history:
Received 22 December 2016
Received in revised form
21 June 2017
Accepted 11 July 2017
Available online 17 July 2017

Keywords:
Ultrafast spectroscopy
Protoporphyrin IX
Nanohybrid
Visible light photocatalysis and DSSC

ABSTRACT

Nanomaterials and nanohybrids hold promising potency to enhance the performance of photovoltaic as well as photocatalytic efficiency by improving both light trapping and photo-carrier collection. In the present study, we have synthesized Protoporphyrin IX-Titanium dioxide (PP-TiO_2) nanohybrid as a model light harvesting nanohybrid for potential applications in photovoltaics and photocatalytic devices. We observed that the light harvesting nanohybrid shows efficient photocatalytic activity when copper (II) ion is centrally located within the porphyrin moiety. In contrast, presence of copper (II) ion within the porphyrin moiety decreases photovoltaic efficiencies. High-resolution transmission electron microscopy (HRTEM), X-ray diffraction (XRD), and steady-state absorption and emission spectroscopies have been used to analyze the structural details and optical properties of this nanohybrid. Time-resolved fluorescence technique has been applied to study the ultrafast dynamics which is key to photocatalytic and photovoltaic activities. The reason behind the outstanding photocatalytic performance of the nanohybrid after copper metalation, is found to have additional stability against photobleaching while enhanced back electron transfer after copper metalation decreases its photovoltaic efficiency.

1. Introduction

Recently, use of solar harvesting nanomaterials is found to be important to improve photocatalysis and dye sensitized solar cells efficiencies taking full advantage of the main part of the solar

* Corresponding author.
E-mail address: skpal@bose.res.in (S.K. Pal).

http://dx.doi.org/10.1016/j.matchemphys.2017.07.042
0254-0584/

spectrum [1–8]. However, practical applications of the nanomaterials have been limited because of a serious drawback due to several interfacial dynamical processes at the interface of the sensitizer and host semiconductor [9–12]. It is well-known that the electron transfer on the interface between the sensitizer and the semiconductor is of great significance to the photocatalytic and photovoltaic efficiencies [13–16]. Thus, efficient electron transfer at the interface due to coupling between the sensitizer and semiconductor cause a rapid photoinduced charge separation and a relatively slow charge recombination, and hence an improved efficiency of solar energy harvesting can be achieved [17,18]. Therefore, study of interfacial carrier dynamics of light harvesting nanohybrid is very much important in order to understand the alteration of photocatalysis and photovoltaic efficiencies. Yang et al. developed an organic-inorganic hybrid material where interfacial charge separation between TiO_2 and conjugated structure facilitates to improve the photocatalytic efficiency [19]. In this direction, extensive efforts have been devoted like metal-ion doping, nonmetal doping, noble metal deposition, narrow bandgap semiconductor coupling, conducting polymer sensitization, and dye sensitization to modify the semiconductor in order to get better light harvesting ability [20–25]. In one of our recent studies, we have developed an efficient light harvesting heterostructure based on poly(diphenylbutadiyne) (PDPB) nanofibers and ZnO nanoparticles which is helpful in photocatalysis [26]. Previously, we sensitized ZnO nanorods with hematoporphyrin which exhibit twin applications in efficient visible light photocatalysis and dye sensitized solar cell [27]. We have also demonstrated how presence of naturally abundant iron(III) and copper(II) ions significantly alter visible light photocatalytic activity of PP-ZnO nanohybrid [23]. Recently, we have shown dipolar coupling between porphyrin and plasmonic nanoparticles facilitates enhanced solar energy conversation when they are embedded on a host semiconductor matrix [28]. Towards this direction, nanohybrid systems seem to be ideal to achieve enhanced light-harvesting and charge-transfer which is usually helpful to get better solar energy conversion.

Porphyrin, a well known photosensitizer has been extensively used as a light harvesting material upon sensitization with semiconductor due to low cost, low toxicity and environmental compatibility compared to ruthenium-based inorganic dyes [29–32]. Thus, porphyrin based light harvesting nanomaterials have a wide application in photocatalysis, dye sensitized solar cell, photodynamic therapy [28,33–35]. In our previous study, we observed that attachment of Protoporphyrin with ZnO nanoparticles has a potential application in drug delivery vehicle of cancer drugs [33]. Nolan et al. showed that tetra(4-carboxyphenyl)porphyrin (TCPP)–TiO_2 composite is very much efficient in the photo-degradation of the pharmaceuticals [36]. However, to the best of our knowledge, effect of interfacial carrier dynamics in dual application of photovoltaic and photocatalysis using same porphyrin based light harvesting nanohybrid are sparse in the existing literature and one of our motives in this present work.

In the present study, we have synthesized Protoporphyrin IX-Titanium dioxide (PP-TiO_2) nanohybrid as a model light harvesting nanohybrid for potential applications in photovoltaics and photocatalytic devices. We observed that the presence of Cu (II) ion within the porphyrin moiety of the nanohybrid can alter overall photocatalytic and photovoltaic activity. Picosecond-resolved fluorescence studies of the nanohybrids in the absence and presence of metal ion have been employed to investigate the ultrafast interfacial charge transfer dynamics upon photoexcitation. We have further investigated that presence of copper within porphyrin moiety shows excellent photocatalytic activity for the degradation of Methylene Blue (MB) used as a model organic pollutant. We have fabricated DSSCs with the nanohybrid which exhibit much lower power conversation efficiencies compared to their counterparts.

2. Experimental section

2.1. Reagents

TiO_2, protoporphyrin IX (PP), methylene blue (MB), platinum chloride (H_2PtCl_6), lithium iodide (LiI), iodine (I_2) and 4-*tert*-butylpyridine (TBP) were purchased from Sigma-Aldrich. Ultrapure water (Millipore System, 18.2 MΩ cm) and ethanol (≥99% for HPLC, purchased from Sigma-Aldrich) were used as solvents. All other chemicals used in the study were of analytical grade and were used without further purification. Fluorine-doped tin oxide (FTO) conducting glass substrates, acquired from Sigma-Aldrich were cleaned by successive sonication with soap water, acetone, deionized (DI) water, and ethanol for 20 min, each with adequate drying prior to their use.

2.2. Sensitization of TiO_2 with PP and Cu(II)PP

A 0.5 mM PP ($C_{34}H_{36}N_4O_5$) solution was prepared in dimethyl sulfoxide (DMSO) under constant stirring for 1 h. Sensitization of PP with TiO_2 nanoparticles was done by addition of TiO_2 nanoparticles into PP followed by overnight stirring. Next, the nanohybrid was filtered out and washed several times with DMSO in order to remove unbound PP. Finally, as synthesized nanohybrid was dried in an oven and put in dark until further use. The synthesis of Cu(II) PP was carried by addition of 1:1 PP (0.5 mM) and copper sulphate pentahydrate ($CuSO_4 \cdot 5H_2O$) followed by overnight stirring. Next sensitization with TiO_2 nanoparticles was performed in the similar method as described above.

2.3. Characterization methods

Transmission electron microscopy (TEM) grids were prepared by applying a diluted drop of the samples to carbon-coated copper grids. The particle sizes were determined from micrographs recorded at a magnification of 100000× using an FEI (Technai S-Twin, operating at 200 kV) instrument. X-ray diffraction (XRD) patterns of the samples were recorded by employing a scanning rate of 0.02° S^{-1} in the 2θ range from 20° to 80° using a PANalytical XPERTPRO diffractometer equipped with Cu Kα radiation (at 40 mA and 40 kV). For optical experiments, the steady-state absorption and emission were carried out with a Shimadzu UV-2600 spectrophotometer and a Jobin Yvon Fluoromax-3 fluorimeter, respectively. FTIR spectra were recorded on a JASCO FTIR-6300 spectrometer, using a CaF_2 window. The current density-voltage characteristics of the cells were recorded by Keithley under an irradiance of 100 mW cm^{-2} (AM 1.5 simulated illuminations, Photo Emission Tech). The wavelength-dependent photocurrent is measured using a homemade setup with a Bentham monochromator and dual light (tungsten and xenon) sources. Photovoltage decay measurements were carried out after illuminating the cells under 1 Sun. The photovoltage decays after switching off the irradiation were monitored by an oscilloscope (Owon) through computer interface. The decays were fitted with exponential decay functions using origin software. For steady state and time resolved optical studies, we have followed the methodology as described in our earlier work [23,37].

2.4. Fabrication of DSSCs

For the fabrication of DSSCs, at first TiO_2 paste was coated on a FTO glass substrate. The photoanode was annealed at 450 °C for 1 h. After that photoanode were immersed in a 0.5 mM PP, (Cu)PP solutions separately for 24 h at room temperature. For preparation of

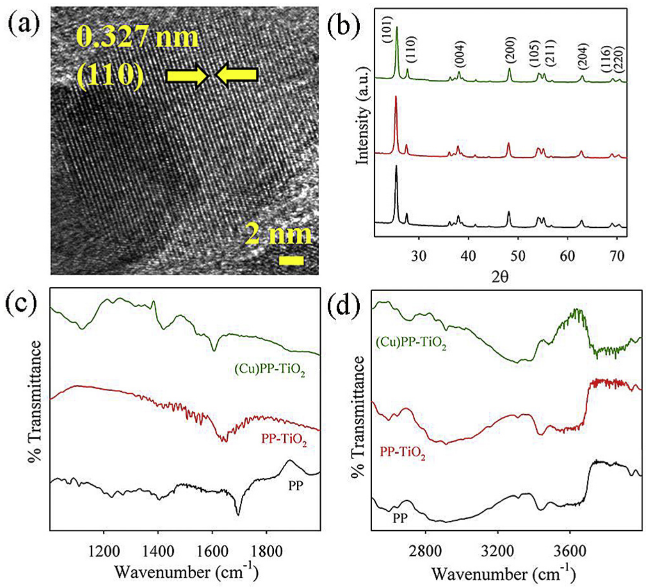

Fig. 1. (a) HRTEM images of TiO_2 NPs. (b) X-ray diffraction patterns of TiO_2, PP-TiO_2 and (Cu)PP-TiO_2. (c) FTIR spectra of PP, PP-TiO_2 and (Cu)PP-TiO_2. (d) FTIR spectra of PP, PP-TiO_2, and (Cu)PP-TiO_2.

counter electrode, the platinum (Pt) was deposited on the FTO substrates by thermal decomposition of 10 mM platinum chloride (in isopropanol) at 385 °C for 30 min. The two electrodes were placed on top of each other with a single layer of 60 μm thick Surlyn (Solaronix) as a spacer between the two electrodes. A liquid electrolyte composed of 0.5 M lithium iodide (LiI), 0.05 M iodine (I_2) and 0.5 M 4-*tert*-butylpyridine (TBP) in acetonitrile was used as the hole conductor and filled in the inter electrode space by using capillary force, through two small holes (diameter = 1 mm) predrilled on the counter electrode. Finally, the two holes were sealed by using another piece of Surlyn to prevent the leakage of electrolyte from the cell. In all our experiments, the active area of the DSSCs was fixed at 0.64 cm^2.

2.5. Photocatalytic performance measurements

The photocatalytic activity of the samples were evaluated in terms of photodegradation of methylene blue (MB) taken as a model pollutant in water. The photodegradation reaction of MB (initial concentration $C_0 = 0.5 \times 10^{-5}$ M) was carried out in a 10 mm optical path quartz cell reactor containing 2 mL of a model MB solution with a concentration of 0.5 g L^{-1} of the photocatalyst in deionized water (DI). The suspension was irradiated with a mercury lamp, $\lambda \geq 400$ nm (under Visible light) and absorbance data were collected continuously by UV–Vis spectroscopy. The percentage degradation (% DE) of MB was determined using Equation:

$$\%\,DE = \frac{I_0 - I}{I_0} \times 100 \qquad (1)$$

where I_0 is the initial absorption intensity of MB at $\lambda_{max} = 660$ nm and I is the absorption intensity after irradiation.

3. Results and discussion

Fig. 1a shows the HRTEM image of the TiO_2 nanoparticles. The average size of TiO_2 nanoparticle was found to be 25 nm. The HRTEM image of TiO_2 nanoparticles shows the high crystallinity of the nanoparticles. The inter-planar distance between the fringes is found to be about 0.327 nm which is consistent with (110) planes of bulk TiO_2 [38]. The X-ray diffraction patterns (As shown in Fig. 1b) indicate that there is no significant change in the 2θ angle of the signals for the sensitized TiO_2 nanohybrids compared to the unmodified TiO_2. Intactness of the crystal planes of TiO_2 upon sensitization with PP and Cu(II)PP also evident from this study. Fourier-transform infrared (FTIR) spectroscopy was used to confirm the binding mode of PP on the TiO_2 surface. For free PP, stretching frequencies of the carboxylic group are located at 1696 and 1402 cm^{-1} for the antisymmetric and symmetric stretching vibrations, respectively, as shown in Fig. 1c. In PP-TiO_2, the perturbation of stretching frequencies of the carboxylic groups providing clear evidence for binding of the carboxylic groups with TiO_2 NPs. The difference in stretching frequencies, $\Delta = \gamma_{as} - \gamma_{sym}$ is a useful parameter in identifying the binding mode of the carboxylate ligand [39]. For PP-TiO_2 nanohybrid, the observed Δ value (198 cm^{-1}) is found to be smaller compared to free PP (294 cm^{-1}) which indicates that the binding mode of PP on TiO_2 is bidentate in nature. Similar bidentate covalent binding of (Cu)PP with TiO_2 is also observed from FTIR study. The perturbation of *N*-H stretching frequency confirms the successful metalation within the porphyrin moiety. In the presence of Cu (II) ion, the stretching frequency of *N*-H bond is perturbed (as

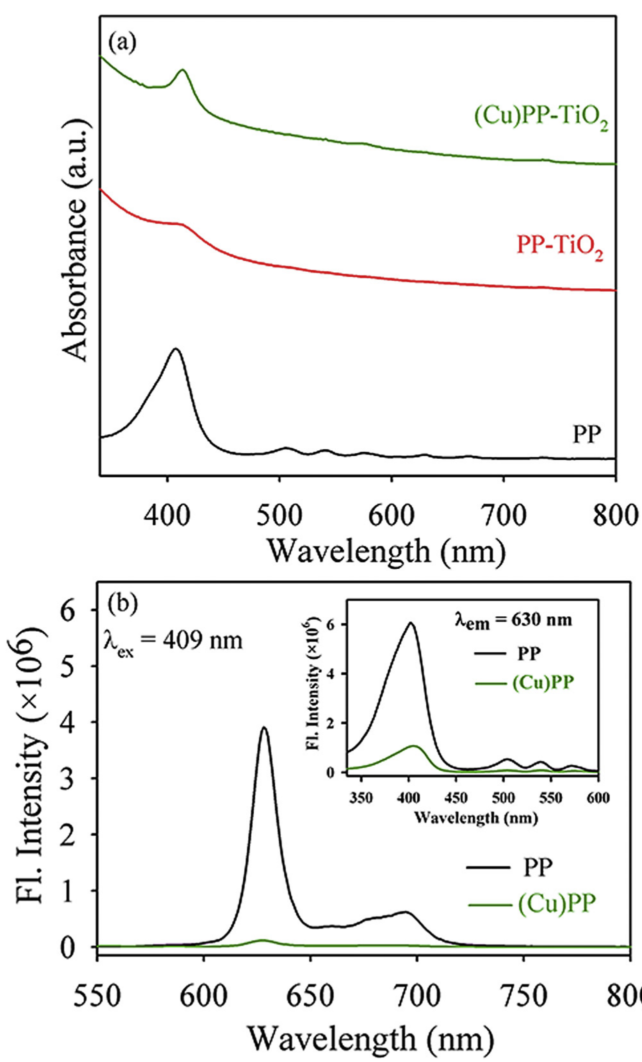

Fig. 2. (a) UV-Vis absorption spectra of PP, PP-TiO_2 and (Cu)PP-TiO_2. (b) Room temperature fluorescence spectra of PP and (Cu)PP. The inset shows excitation spectra monitored at 630 nm.

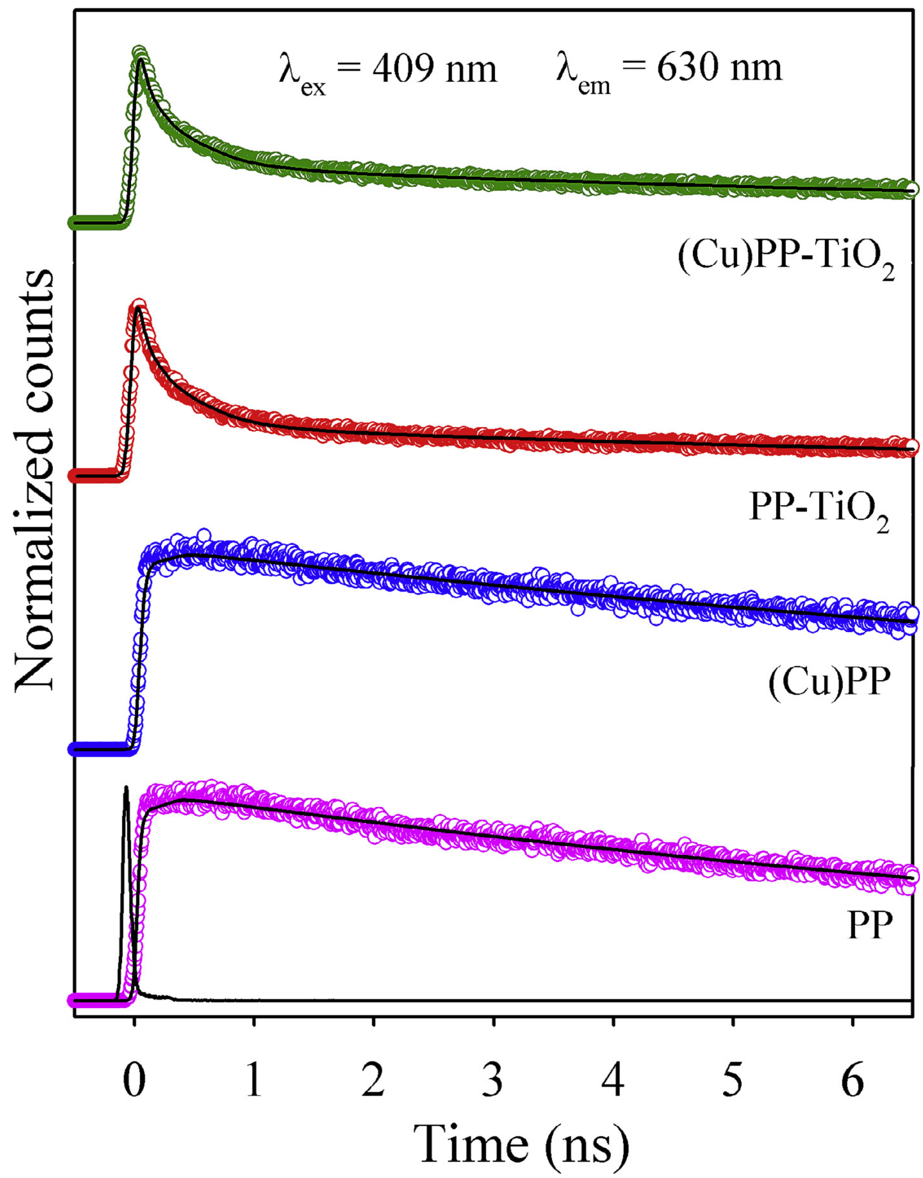

Fig. 3. Fluorescence decay profiles of PP, (Cu)PP, PP-TiO_2, and (Cu)PP- TiO_2 measured at 630 nm wavelength upon excitation at a wavelength of 409 nm.

shown in Fig. 1d), which indicates the binding of Cu (II) ion with the pyrrole nitrogen atoms of the PP [23].

The structure of PP has extensive delocalized π electrons which exhibits a Soret band (405 nm) and Q bands (500–700 nm) due to its $\pi-\pi^*$ electronic transitions [40,41]. The PP–TiO_2 nanohybrid exhibits a 5 nm bathochromic shift of the Soret band compare to the absorption of PP as shown in Fig. 2a. Such bathochromic shift signifies different changes within the porphyrin molecules upon attachment with a solid surface. Kar et al. have proposed a 16 nm red shift in the absorption of PP molecule upon attachment with ZnO nanoparticles [23]. Sarkar et al. demonstrated that attachment of Hematoporphyrin molecule with TiO_2 nanoparticles exhibits a 3 nm bathochromic shift [27]. However, after metalation with copper (II) ion, steady-state emission of PP is significantly decreased (as shown in Fig. 2b), indicating non-radiative processes that can be attributed to fast intersystem crossing to the excited triplet state. Kim et al. also reported a several charge transfer transitions which are responsible for the quenching of the emission of PP [42].

Table 1
Lifetimes of picosecond time-resolved PL transients of PP, PP-TiO_2 and (Cu)PP-TiO_2 detected at 630 nm PL maxima uopn excitation at 409 nm wavelength. The values in parentheses represent the relative weight percentages of the time components.

System	τ_1 (ps)	τ_2 (ps)	τ_3 (ps)	τ_{avg} (ns)
PP	11300 (100%)			11.3
(Cu)PP	11400(100%)			11.4
PP-TiO_2	300(59%)	9800(41%)		4.2
(Cu)PP-TiO_2	300(57%)	9712(43%)		4.3

Picosecond resolved emission transients have been used in order to investigate the excited state electron transfer dynamics of the nanohybrids [17,34]. The fluorescence decay of PP, (Cu)PP, PP-TiO_2 and (Cu)PP-TiO_2 are shown in Fig. 3 and associated time constant value are tabulated in Table 1. The average life time of both PP and (Cu)PP have comparable timescale. Thus excited state electron transfer from PP to Cu (II) ion is ruled out from our Picosecond-resolved fluorescence data. However, decrease in average life time was observed for PP-TiO_2 in compare to PP and (Cu)PP. This is due to a significant faster component (200 ps) in case of PP-TiO_2 compare to PP showing excited state electron transfer from PP to TiO_2. Presence

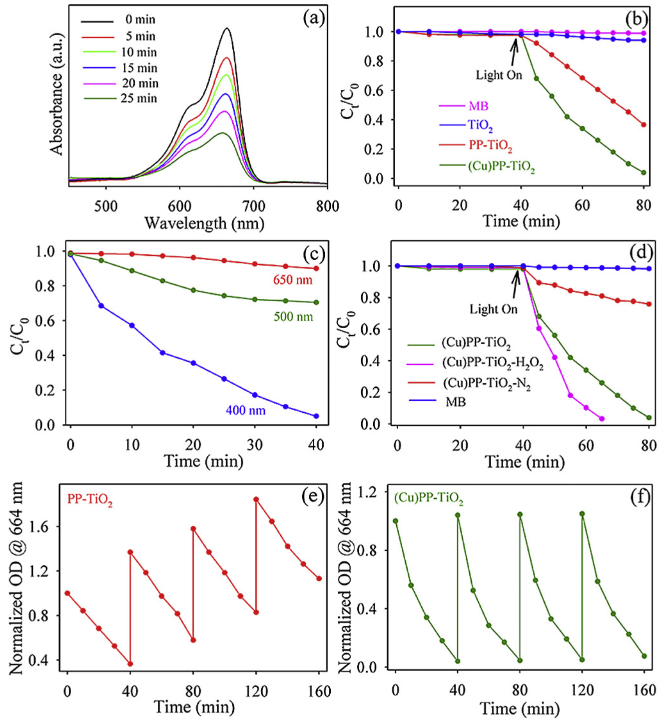

Fig. 4. (a) UV–Vis spectra for degradation of MB under visible light illumination by (Cu)PP-TiO_2. (b) Photocatalytic degradation of MB in presence of TiO_2, PP-TiO_2 and (Cu) PP-TiO_2 and only MB under visible light illumination. (c) Photocatalytic degradation of MB by (Cu)PP-TiO_2 at different wavelength. (d) Photodegradation of MB by (Cu)PP-TiO_2 under conventional condition, presence of H_2O_2 and N_2 into the solution. A recyclability studies of (e) PP-TiO_2 and (f) (Cu)PP-TiO_2 under visible light illumination are also shown.

of Cu (II) ion within porphyrin moiety the fluorescence decay of (Cu) PP-TiO_2 remain essentially unaltered.

The photocatalytic activities of the nanohybrids were evaluated by photodegradation of the model organic contaminant MB under visible light irradiation. During the photocatalytic reaction, MB forms a well-known colorless product leucomethylene blue (LMB) as shown in Eq. (2) [43,44].

$$2MB + 2e^- + H^+ = MB + LMB \quad (2)$$

Fig. 4a shows the time dependent UV–Vis spectra of MB in presence of the (Cu)PP-TiO_2 nanocomposite in a neutral aqueous solution under visible-light irradiation. Fig. 4b shows changes in MB concentration as a function of time in presence and absence of photocatalysts under visible light irradiation. MB does not undergo decomposition reaction prior to illumination. The direct visible-light illumination without any catalyst is leading to insignificant decomposition of MB molecules within our experimental time window. The pure TiO_2 nanoparticles exhibit <5% degradation of MB under the same conditions. In contrast, PP-TiO_2 shows an enhanced photocatalytic activity: 60% of MB degraded after 60 min illumination. (Cu)PP-TiO_2 nanohybrid showed almost complete degradation of MB (99%) within the same experimental time window. Thus results demonstrate that presence of Cu (II) ion within porphyrin moiety further enhanced photocatalytic activity. The photocatalytic degradation efficiency of the light harvesting nanohybrid i.e. (Cu) PP-TiO_2 is reasonably good compared to the earlier reported literature [45–48]. Fig. 4c shows photocatalysis of methylene blue (MB) at different wavelengths by (Cu)PP-TiO_2. Insignificant photocatalysis at 650 nm (MB absorbance maxima 660 nm) indicates that MB is unable to photosensitize (Cu)PP-TiO_2. Thus photocatalysis

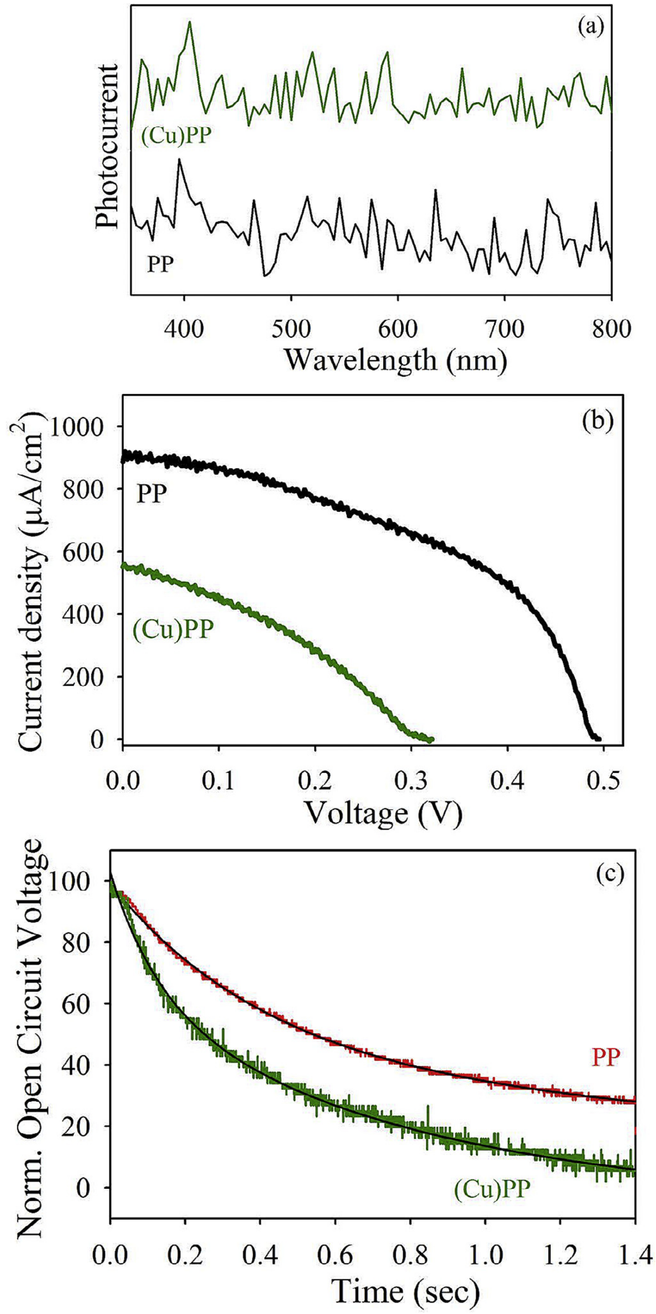

Fig. 5. (a) Wavelength dependent photocurrent response curves of different DSSCs (b) Current density–voltage curves under 100 mW cm^{-2} simulated AM 1.5G solar light irradiation. (c) Open circuit voltage decay profiles of different DSSCs.

predominately takes place via sensitization of (Cu)PP-TiO_2. To explain reasons behind the enhanced photocatalytic behavior of the catalyst and underlying degradation mechanism, we further studied the photocatalytic activity of (Cu)PP-TiO_2 in the presence of a radical

Table 2
Photovoltaic performance of DSSCs in presence and absence of copper ion within the protoporphyrin macrocycle.

Cell	J_{SC} (μA/cm^2)	V_{OC} (V)	FF (%)	Efficiency (%)
PP-TiO_2	885.94	0.50	47.19	0.21
(Cu)PP-TiO_2	550.55	0.32	34.17	0.05

Table 3
Dynamics of photovoltage transients of DSSCs fabricated using different active electrodes. The values in parentheses represent the relative weight percentages of the time components.

Active electrode	τ_1 (ms)	τ_2 (ms)	τ_{avg} (s)
PP-TiO_2	0.42(63.1%)	3.0(36.9%)	1.37
(Cu)PP-TiO_2	0.13(36.4%)	0.76(63.6%)	0.53

initiator (H_2O_2) and radical quencher (N_2 bubbling) separately (Fig. 4d). Radical initiator and radical scavenger experiments were carried out to confirm the dominance of active species involved in the degradation process [49]. In fact, in the presence of H_2O_2, increases generation of OH· under solar light illumination which eventually increases the photocatalytic activity of (Cu)PP-TiO_2 for degradation of MB. The observation demonstrates the role of reactive oxygen species (ROS) in the degradation of MB. We further observed that the photodegradation efficiency of (Cu)PP-TiO_2 decreases with N_2 bubbling in the solution. The result implies that O_2 primarily acts as an efficient electron trap, leading to the generation of $O_2^{\bullet-}$ radicals during photocatalytic reaction [50]. Under visible light irradiation, the sensitizer (PP) injects electrons into the conduction band (CB) of TiO_2 and the subsequent degradation of MB takes place is initiated by CB electrons being transferred to it through reactive oxygen species (ROS). From the application point of view, photochemical stability and photocorrosion of the photocatalysts are also important parameters for evaluating their performance as it could reduces the cost of the process appreciably during photocatalytic reaction [51–53]. In order to further study photocatalytic performance of the as prepared nanohybrids, recycling experiment was carried out under repeated irradiation. Fig. 5e–f shows the repeated photocatalytic activity of different nanohybrids. The results indicate that there is insignificant decrease about the photodegradation efficiency for the CuPP-TiO_2 rate, which remains similar after four consecutive cycles, implying highest stability of the catalyst during the photodegradation of MB. On the other hand, after four cycles, photocatalytic activity reduced to 30% (PP-TiO_2). The relatively efficient photocatalysis by the (Cu)PP-TiO_2 nanohybrid may be correlated with the additional structural stability due to presence of copper ion within the PP moiety [46,54,55]. The results also demonstrate that CuPP-TiO_2 is highly stable photocatalyst for practical application.

The light-harvesting ability of a sensitizer is a key parameter that determines the ability of solar energy capture and thus affects the photocurrent generated by the solar cell [56,57]. The photocurrent measurements on the fabricated PP-TiO_2 and (Cu)PP-TiO_2 DSSC are shown in Fig. 5a. The photocurrent spectra are found to be closely resembled with the absorption spectra of PP. The observation demonstrated that PP sensitizers on the photoanode surface are indeed responsible for photocurrent generation. In order to investigate the photovoltaic performance, we have fabricated DSSCs based on the porphyrin sensitizers. The J–V characteristics of the PP–TiO_2 DSSC with Cu (II) as central metal are shown in Fig. 5b. The solar cell parameters are shown in Table 2. The results demonstrated that presence of copper within the porphyrin moiety decreases overall photovoltaic efficiency. Different photovoltaic efficiency in presence of Cu (II) ion within the porphyrin moiety have been investigated by monitoring the temporal decay of the open circuit voltage which has been monitored for different cells in the dark following a brief period of illumination as shown in Fig. 5c. The open circuit voltage decay reflects the timescales (as shown in Table 3) for the recombination processes of the electrons at the conduction band of the semiconductor with the oxidized electrolytes. Inclusion of copper within the porphyrin moiety eventually increase the back electron transfer, thus can substantially affect the photovoltaic performance i.e. reduces its efficiency [28,58,59].

There are several reports which indicate that a promising light harvesting nanohybrid is very much efficient for photocatalysis and photovoltaic applications due to synergetic effect of many factors like hierarchical structure, surface area, rapid photoinduced charge separation and a relatively slow charge recombination [60–63]. In our present study, the developed PP-TiO_2 light harvesting nanohybrid is very much efficient for MB degradation in presence of Cu (II) ion within the core of porphyrin moiety. A tentative photocatalytic mechanism of (Cu)PP-TiO_2 was deduced and a schematic illustration shown in Scheme 1. Under visible light illumination, excitation of electron from HOMO to LUMO takes place by PP molecule attached on TiO_2 surface. Then transfer of electron to the CB of TiO_2 takes place which eventually reacts with dissolve oxygen and water to produce ROS. However, presence of Cu (II) ion within

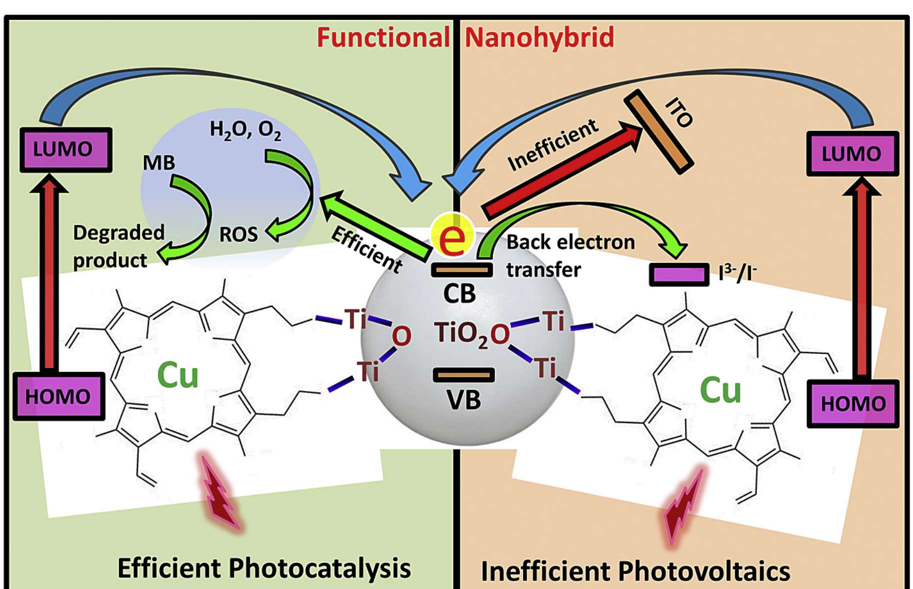

Scheme 1. Schematic representation of the overall mechanistic pathways for photocatalytic and photovoltaic efficiency by (Cu)PP-TiO_2 (see text).

porphyrin moiety increases stability of (Cu)PP-TiO_2 nanohybrid against photo bleaching and thus promote generation of ROS that are responsible for enhancement in photocatalytic activity. To further study the effect on photovoltaics by (Cu)PP-TiO_2 nanohybrid, we observed that light harvesting nanohybrid is inefficient for DSSC application. We note that although nanohybrid is sufficiently stable against photobleaching, the enhanced back electron transfer due to the recombination of photoinjected electrons at the CB of TiO_2 with redox electrolyte contribute significantly. The enhancement in back electron transfer is therefore responsible for poor photovoltaic device as it diminish the charge carriers to be collected into their respective contacts. Based on the above observation a schematic illustration is proposed as shown in Scheme 1.

4. Conclusion

In the present study, PP-TiO_2 has been used as a light harvesting nanohybrid for photocatalysis and DSSCs application. The picosecond resolved fluorescence quenching successfully explains the excited state electron transfer dynamics in the nanohybrid. In the Protoporphyrin sensitizers, the presence of centrally located Cu (II) ion can substantially affect the photovoltaic and photocatalytic performance. Presence of copper ion within the porphyrin moiety increases the photocatalytic activity but decreases the DSSC efficiency. The outstanding photocatalytic activity of the (Cu)PP-TiO_2 nanohybrid is concluded to be structural stability, whereas faster back electron transfer is found to be responsible for poor photovoltaic performance. These results highlight that different ultrafast processes are equally crucial in light harvesting nanohybrid upon photoinduced charge separation. The present work also demonstrates that exciting potential light harvesting nanohybrid may not always simultaneously be used in visible-light photocatalysis and photovoltaics.

Acknowledgements

P·K., J.P. thanks Council of Scientific and Industrial Research (CSIR, India) for fellowship. T.K.M. thanks of DST, INSPIRE for fellowship. We thank DST, India for financial grants (DST-TM-SERI-FR-117, EMR/2016/004698). We also thank DAE (India) for financial grant 2013/37P/73/BRNS.

References

[1] Z. Abdin, M.A. Alim, R. Saidur, M.R. Islam, W. Rashmi, S. Mekhilef, A. Wadi, Solar energy harvesting with the application of nanotechnology, Renew. Sustain. Energy Rev. 26 (2013) 837–852.
[2] Z.L. Wang, W. Wu, Nanotechnology-enabled energy harvesting for self-powered micro-/nanosystems, Angew. Chem. Int. Ed. 51 (2012) 11700–11721.
[3] Y. Bai, I. Mora-Seró, F. De Angelis, J. Bisquert, P. Wang, Titanium dioxide nanomaterials for photovoltaic applications, Chem. Rev. 114 (2014) 10095–10130.
[4] R. Yu, Q. Lin, S.-F. Leung, Z. Fan, Nanomaterials and nanostructures for efficient light absorption and photovoltaics, Nano Energy 1 (2012) 57–72.
[5] R. Slota, G. Dyrda, K. Szczegot, G. Mele, I. Pio, Photocatalytic activity of nano and microcrystalline TiO2 hybrid systems involving phthalocyanine or porphyrin sensitizers, Photochem. Photobiol. Sci. 10 (2011) 361–366.
[6] Y. Shen, X. Yu, W. Lin, Y. Zhu, Y. Zhang, A facile preparation of immobilized BiOCl nanosheets/TiO2 arrays on FTO with enhanced photocatalytic activity and reusability, Appl. Surf. Sci. 399 (2017) 67–76.
[7] C.-K. Huang, T. Wu, C.-W. Huang, C.-Y. Lai, M.-Y. Wu, Y.-W. Lin, Enhanced photocatalytic performance of BiVO4 in aqueous AgNO3 solution under visible light irradiation, Appl. Surf. Sci. 399 (2017) 10–19.
[8] J. Lv, D. Li, K. Dai, C. Liang, D. Jiang, L. Lu, G. Zhu, Multi-walled carbon nanotube supported CdS-DETA nanocomposite for efficient visible light photocatalysis, Mater. Chem. Phys. 186 (2017) 372–381.
[9] J.Z. Zhang, Interfacial charge carrier dynamics of colloidal semiconductor nanoparticles, J. Phys. Chem. B 104 (2000) 7239–7253.
[10] A. Listorti, B. O'Regan, J.R. Durrant, Electron transfer dynamics in dye-sensitized solar cells, Chem. Mater. 23 (2011) 3381–3399.
[11] P. Tiwana, P. Docampo, M.B. Johnston, H.J. Snaith, L.M. Herz, Electron mobility and injection dynamics in mesoporous ZnO, SnO2, and TiO2 films used in dye-sensitized solar cells, ACS Nano 5 (2011) 5158–5166.
[12] T.K. Maji, D. Bagchi, P. Kar, D. Karmakar, S.K. Pal, Enhanced charge separation through modulation of defect-state in wide band-gap semiconductor for potential photocatalysis application: ultrafast spectroscopy and computational studies, J. Photochem. Photobiol. A 332 (2017) 391–398.
[13] S. Meng, E. Kaxiras, Electron and hole dynamics in dye-sensitized solar cells: influencing factors and systematic trends, Nano Lett. 10 (2010) 1238–1247.
[14] J.Z. Zhang, Ultrafast studies of electron dynamics in semiconductor and metal colloidal Nanoparticles: effects of size and surface, Acc. Chem. Res. 30 (1997) 423–429.
[15] S. Sardar, S. Sarkar, M.T.Z. Myint, S. Al-Harthi, J. Dutta, S.K. Pal, Role of central metal ions in hematoporphyrin-functionalized titania in solar energy conversion dynamics, Phys. Chem. Chem. Phys. 15 (2013) 18562–18570.
[16] R.L. Milot, C.A. Schmuttenmaer, Electron injection dynamics in high-potential porphyrin photoanodes, Acc. Chem. Res. 48 (2015) 1423–1431.
[17] S. Sarkar, A. Makhal, T. Bora, S. Baruah, J. Dutta, S.K. Pal, Photoselective excited state dynamics in ZnO-Au nanocomposites and their implications in photocatalysis and dye-sensitized solar cells, Phys. Chem. Chem. Phys. 13 (2011) 12488–12496.
[18] S.A. Haque, E. Palomares, B.M. Cho, A.N.M. Green, N. Hirata, D.R. Klug, J.R. Durrant, Charge separation versus recombination in dye-sensitized nanocrystalline solar Cells: the minimization of kinetic redundancy, J. Am. Chem. Soc. 127 (2005) 3456–3462.
[19] P. Lei, F. Wang, S. Zhang, Y. Ding, J. Zhao, M. Yang, Conjugation-Grafted-TiO2 nanohybrid for high photocatalytic efficiency under visible light, ACS Appl. Mater. Interfaces 6 (2014) 2370–2376.
[20] H. Li, Z. Bian, J. Zhu, Y. Huo, H. Li, Y. Lu, Mesoporous Au/TiO2 nanocomposites with enhanced photocatalytic activity, J. Am. Chem. Soc. 129 (2007) 4538–4539.
[21] J.C. Yu, Yu, Ho, Jiang, Zhang, Effects of F- doping on the photocatalytic activity and microstructures of nanocrystalline TiO2 powders, Chem. Mater. 14 (2002) 3808–3816.
[22] K. Selvam, M. Swaminathan, Au-doped TiO2 nanoparticles for selective photocatalytic synthesis of quinaldines from anilines in ethanol, Tetrahedron Lett. 51 (2010) 4911–4914.
[23] P. Kar, S. Sardar, E. Alarousu, J. Sun, Z.S. Seddigi, S.A. Ahmed, E.Y. Danish, O.F. Mohammed, S.K. Pal, Impact of metal ions in porphyrin-based applied materials for visible-light photocatalysis: key information from ultrafast electronic spectroscopy, Chem. Eur. J. 20 (2014) 10475–10483.
[24] R. Qiu, D. Zhang, Z. Diao, X. Huang, C. He, J.-L. Morel, Y. Xiong, Visible light induced photocatalytic reduction of Cr(VI) over polymer-sensitized TiO2 and its synergism with phenol oxidation, Water Res. 46 (2012) 2299–2306.
[25] N. Liang, M. Wang, L. Jin, S. Huang, W. Chen, M. Xu, Q. He, J. Zai, N. Fang, X. Qian, Highly efficient Ag2O/Bi2O2CO3 p-n heterojunction photocatalysts with improved visible-light responsive activity, ACS Appl. Mater. Interfaces 6 (2014) 11698–11705.
[26] S. Sardar, P. Kar, H. Remita, B. Liu, P. Lemmens, S. Kumar Pal, S. Ghosh, Enhanced charge separation and FRET at heterojunctions between semiconductor nanoparticles and conducting polymer nanofibers for efficient solar light harvesting, Sci. Rep. 5 (2015) 17313.
[27] S. Sarkar, A. Makhal, T. Bora, K. Lakhsman, A. Singha, J. Dutta, S.K. Pal, Hematoporphyrin–ZnO nanohybrids: twin applications in efficient visible-light photocatalysis and dye-sensitized solar cells, ACS Appl. Mater. Interfaces 4 (2012) 7027–7035.
[28] P. Kar, T.K. Maji, P.K. Sarkar, S. Sardar, S.K. Pal, Direct observation of electronic transition-plasmon coupling for enhanced electron injection in dye-sensitized solar cells, RSC Adv. 6 (2016) 98753–98760.
[29] L.M. Peter, The Grätzel cell: where next? J. Phys. Chem. Lett. 2 (2011) 1861–1867.
[30] R. Bonnett, Photosensitizers of the porphyrin and phthalocyanine series for photodynamic therapy, Chem. Soc. Rev. 24 (1995) 19–33.
[31] M. Silva, M.E. Azenha, M.M. Pereira, H.D. Burrows, M. Sarakha, C. Forano, M.F. Ribeiro, A. Fernandes, Immobilization of halogenated porphyrins and their copper complexes in MCM-41: environmentally friendly photocatalysts for the degradation of pesticides, Appl. Catal. B 100 (2010) 1–9.
[32] A. Suzuki, K. Kobayashi, T. Oku, K. Kikuchi, Fabrication and characterization of porphyrin dye-sensitized solar cells, Mater. Chem. Phys. 129 (2011) 236–241.
[33] S. Sardar, S. Chaudhuri, P. Kar, S. Sarkar, P. Lemmens, S.K. Pal, Direct observation of key photoinduced dynamics in a potential nano-delivery vehicle of cancer drugs, Phys. Chem. Chem. Phys. 17 (2015) 166–177.
[34] S. Sardar, P. Kar, S.K. Pal, The impact of central metal ions in porphyrin functionalized ZnO/TiO2 for enhanced solar energy conversion, J. Mat. Nanosci. 1 (2014) 12–30.
[35] D. Chen, D. Yang, J. Geng, J. Zhu, Z. Jiang, Improving visible-light photocatalytic activity of N-doped TiO2 nanoparticles via sensitization by Zn porphyrin, Appl. Surf. Sci. 255 (2008) 2879–2884.
[36] S. Murphy, C. Saurel, A. Morrissey, J. Tobin, M. Oelgemöller, K. Nolan, Photocatalytic activity of a porphyrin/TiO2 composite in the degradation of pharmaceuticals, Appl. Catal. B 119–120 (2012) 156–165.
[37] P.K. Sarkar, N. Polley, S. Chakrabarti, P. Lemmens, S.K. Pal, Nanosurface energy transfer based highly selective and ultrasensitive "turn on" fluorescence mercury sensor, ACS Sens. 1 (2016) 789–797.
[38] W.-K. Wang, J.-J. Chen, X. Zhang, Y.-X. Huang, W.-W. Li, H.-Q. Yu, Self-induced

synthesis of phase-junction TiO2 with a tailored rutile to anatase ratio below phase transition temperature, Sci. Rep. 6 (2016) 20491.
[39] G.B. Deacon, R.J. Phillips, Relationships between the carbon-oxygen stretching frequencies of carboxylato complexes and the type of carboxylate coordination, Coord. Chem. Rev. 33 (1980) 227–250.
[40] T.D. Schladt, K. Schneider, M.I. Shukoor, F. Natalio, H. Bauer, M.N. Tahir, S. Weber, L.M. Schreiber, H.C. Schroder, W.E.G. Muller, W. Tremel, Highly soluble multifunctional MnO nanoparticles for simultaneous optical and MRI imaging and cancer treatment using photodynamic therapy, J. Mater. Chem. 20 (2010) 8297–8304.
[41] A. Marcelli, I. Jelovica Badovinac, N. Orlic, P.R. Salvi, C. Gellini, Excited-state absorption and ultrafast relaxation dynamics of protoporphyrin IX and hemin, Photochem. Photobiol. Sci. 12 (2013) 348–355.
[42] D. Kim, D. Holten, M. Gouterman, Evidence from picosecond transient absorption and kinetic studies of charge-transfer states in copper(II) porphyrins, J. Am. Chem. Soc. 106 (1984) 2793–2798.
[43] P. Kar, S. Sardar, S. Ghosh, M.R. Parida, B. Liu, O.F. Mohammed, P. Lemmens, S.K. Pal, Nano surface engineering of Mn2O3 for potential light-harvesting application, J. Mater. Chem. C 3 (2015) 8200–8211.
[44] C. Yogi, K. Kojima, N. Wada, H. Tokumoto, T. Takai, T. Mizoguchi, H. Tamiaki, Photocatalytic degradation of methylene blue by TiO2 film and Au particles-TiO2 composite film, Thin Solid Films 516 (2008) 5881–5884.
[45] X.-q. Su, J. Li, Z.-q. Zhang, M.-m. Yu, L. Yuan, Cu(II) porphyrins modified TiO2 photocatalysts: accumulated patterns of Cu(II) porphyrin molecules on the surface of TiO2 and influence on photocatalytic activity, J. Alloys Compd. 626 (2015) 252–259.
[46] S. Afzal, W.A. Daoud, S.J. Langford, Photostable self-cleaning cotton by a copper(II) porphyrin/TiO2 visible-light photocatalytic system, ACS Appl. Mater. Interfaces 5 (2013) 4753–4759.
[47] C. Wang, J. Li, G. Mele, M.-y. Duan, X.-f. Lü, L. Palmisano, G. Vasapollo, F.-x. Zhang, The photocatalytic activity of novel, substituted porphyrin/TiO2-based composites, Dyes Pigm. 84 (2010) 183–189.
[48] Y. Luo, J. Li, G.-p. Yao, F.-x. Zhang, Influence of polarity of the peripheral substituents of porphyrin molecules on the photocatalytic activity of Cu(ii) porphyrin modified TiO2 composites, Catal. Sci. Tech. 2 (2012) 841–846.
[49] P. Kar, T.K. Maji, R. Nandi, P. Lemmens, S.K. Pal, In-Situ hydrothermal synthesis of Bi–Bi2O2CO3 heterojunction photocatalyst with enhanced visible light photocatalytic activity, Nano-Micro Lett. 9 (2016) 18.
[50] Y. Park, S.-H. Lee, S.O. Kang, W. Choi, Organic dye-sensitized TiO2 for the redox conversion of water pollutants under visible light, Chem. Commun. 46 (2010) 2477–2479.
[51] Q. Lu, Y. Zhang, S. Liu, Graphene quantum dots enhanced photocatalytic activity of zinc porphyrin toward the degradation of methylene blue under visible-light irradiation, J. Mater. Chem. A 3 (2015) 8552–8558.
[52] F.A. Harraz, A.A. Ismail, S.A. Al-Sayari, A. Al-Hajry, Novel α-Fe2O3/polypyrrole nanocomposite with enhanced photocatalytic performance, J. Photochem. Photobiol. A 299 (2015) 18–24.
[53] S. Li, L. Zhang, H. Wang, Z. Chen, J. Hu, K. Xu, J. Liu, Ta3N5-Pt nonwoven cloth with hierarchical nanopores as efficient and easily recyclable macroscale photocatalysts, Sci. Rep. 4 (2014) 3978.
[54] M.-M. Yu, C. Wang, J. Li, L. Yuan, W.-J. Sun, Facile fabrication of CuPp–TiO2 mesoporous composite: an excellent and robust heterostructure photocatalyst for 4-nitrophenol degradation, Appl. Surf. Sci. 342 (2015) 47–54.
[55] X. Zhao, X. Liu, M. Yu, C. Wang, J. Li, The highly efficient and stable Cu, Co, Zn-porphyrin–TiO2 photocatalysts with heterojunction by using fashioned one-step method, Dyes Pigm. 136 (2017) 648–656.
[56] A. Kathiravan, V. Raghavendra, R. Ashok Kumar, P. Ramamurthy, Protoporphyrin IX on TiO2 electrode: a spectroscopic and photovoltaic investigation, Dyes Pigm. 96 (2013) 196–203.
[57] R.L. Milot, G.F. Moore, R.H. Crabtree, G.W. Brudvig, C.A. Schmuttenmaer, Electron injection dynamics from photoexcited porphyrin dyes into SnO2 and TiO2 nanoparticles, J. Phys. Chem. C 117 (2013) 21662–21670.
[58] H. Choi, Y.-S. Chen, K.G. Stamplecoskie, P.V. Kamat, Boosting the photovoltage of dye-sensitized solar cells with thiolated Gold nanoclusters, J. Phys. Chem. Lett. 6 (2015) 217–223.
[59] E. Palomares, J.N. Clifford, S.A. Haque, T. Lutz, J.R. Durrant, Slow charge recombination in dye-sensitised solar cells (DSSC) using Al2O3 coated nanoporous TiO2 films, Chem. Commun. (2002) 1464–1465.
[60] T. Zhao, J. Zai, M. Xu, Q. Zou, Y. Su, K. Wang, X. Qian, Hierarchical Bi2O2CO3 microspheres with improved visible-light-driven photocatalytic activity, CrystEngComm 13 (2011) 4010–4017.
[61] Y. Zhou, Z. Zhao, F. Wang, K. Cao, D.E. Doronkin, F. Dong, J.-D. Grunwaldt, Facile synthesis of surface N-doped Bi2O2CO3: origin of visible light photocatalytic activity and in situ DRIFTS studies, J. Hazard. Mater. 307 (2016) 163–172.
[62] R. Jiang, B. Li, C. Fang, J. Wang, Metal/semiconductor hybrid nanostructures for plasmon-enhanced applications, Adv. Mater. 26 (2014) 5274–5309.
[63] D.M. Fragua, R. Abargues, P.J. Rodriguez-Canto, J.F. Sanchez-Royo, S. Agouram, J.P. Martinez-Pastor, Au–ZnO nanocomposite films for plasmonic photocatalysis, Adv. Mater. Interf. 2 (2015) 1500156.